HDL-mediated cholesterol uptake and targeting to lipid droplets in adipocytes

Georges Dagher,[1] Nathalie Donne, Christophe Klein, Pascal Ferré, and Isabelle Dugail

INSERM Unité 465, Centre de Recherche Biomédicales des Cordeliers (Université Paris 6), 15 rue de l'Ecole de Médecine, 75270 Paris Cedex 06, France

Abstract **Adipocytes express high levels of the HDL scavenger receptor class B type I in a differentiation-dependent manner. We thus have analyzed the routes of HDL cholesterol trafficking at different phases of adipocyte differentiation in the 3T3-L1 cell line. One novel and salient feature of this paper is the observation of a widespread distribution in the cell cytoplasm of Golgi markers, caveolin-2, and a fluorescent cholesterol analog NBD-cholesterol (NBD-chol), observed in the early phases of adipocyte formation, clearly distinct from that observed in mature fat cells (i.e., with fully formed lipid vesicles). Thus, in cells without visible lipid droplets, Golgi markers (Golgi 58K, Golgin 97, trans-Golgi network 38, Rab 6, and BODIPY-ceramide), caveolin-2, and NBD-chol all colocalize in a widespread distribution in the cell. In contrast, when lipid droplets are fully formed at latter stages, these markers clearly are distributed to distinct cell compartments: a compact juxtanuclear structure for the Golgi markers and caveolin-2, while NDB-chol concentrates in lipid droplets. In addition, disorganization of the Golgi using three different agents (Brefeldin, monensin, and *N*-ethyl-maleimide) drastically reduces NBD-chol uptake at different phases of adipocyte formation, strongly suggesting that the Golgi apparatus plays a critical role in HDL-mediated NBD uptake and routing to lipid droplets.—** Dagher, G., N. Donne, C. Klein, P. Ferré, and I. Dugail. **HDL-mediated cholesterol uptake and targeting to lipid droplets in adipocytes. *J. Lipid Res.* 2003.** 44: **1811–1820.**

Supplementary key words high density lipoprotein • traffic • Golgi complex • caveolin • scavenger receptor class B type I

Cholesterol is a crucial component of cell membranes, and as such plays a key role in the regulation of signal transduction (1) and gene expression (2). The homeostasis of cell cholesterol is maintained through complex mechanisms that imply biosynthesis, uptake, and constant recycling between membranes. Many intracellular organelles take part in the regulation of cholesterol trafficking. Among these, the endosomal lysosomal pathway is involved in the uptake of exogenous cholesterol from LDL; caveolae are engaged in cholesterol trafficking to and from the plasma membrane; the endoplasmic reticulum (ER), where some of the enzymes of the cholesterol biosynthetic pathway reside, is of particular importance because it includes a cell cholesterol sensor system linked to the cleavage activating protein sterol-regulatory element binding proteins (SREBP) system (3); and the Golgi apparatus plays a crucial role in sorting processes (4–7). Recently, previously unrecognized organelles have been identified as new players in cholesterol traffic: the cytoplasmic lipid droplets (8).

The adipocyte is the unique cell type in which triglyceride-rich lipid droplets are present continuously and physiologically in the cytoplasm. Free cholesterol is also found in adipocyte lipid droplets (9, 10). On the other hand, the intracellular distribution of cholesterol between the plasma membrane and the lipid droplet is altered in pathological states such as obesity, as pointed out by previous studies from our laboratory (11). As a signature of this defect, we have shown that the cholesterol-regulated transcription factor SREBP-2 was selectively activated in hypertrophied adipocytes from obese rodents. In addition, we have shown that some metabolic abnormalities that characterize adipocyte dysfunction in obesity can be mimicked in normal fat cells by altering their intracellular cholesterol balance (12). For these reasons, we thought that the adipocyte cell type might provide useful information on the intracellular cholesterol trafficking. We took advantage of the existence of committed adipose cell lines that undergo adipose differentiation in culture to investigate the targeting of cholesterol to lipid droplets. Because adipocytes accumulate cholesterol from exogenous sources and express high levels of the HDL scavenger receptor class B type I (SR-BI) (13, 14), we examined the targeting of an HDL-associated fluorescent cholesterol analog, NBD-cholesterol (NBD-chol), to the lipid droplets at different stages of the adipocyte differentiation program.

The results of this study show that the distribution of

Manuscript received 19 June 2003 and in revised form 1 July 2003.

Published, JLR Papers in Press, July 16, 2003.
DOI 10.1194/jlr.M300267-JLR200

[1] To whom correspondence should be addressed.
e-mail: dagher@ccr.jussieu.fr

the Golgi complex, caveolin-2, and cholesterol exhibit marked changes in distribution during the differentiation process of adipocytes. The Golgi complex and caveolin-2 exhibit a dispersed distribution and colocalization with cholesterol in the first phase of adipocyte formation. In contrast, in fully differentiated lipid laden cells, the Golgi complex, as well as caveolin-2, occupies a juxtanuclear location, while cholesterol distributes preferentially in lipid droplets. These data suggest that the intracellular routes of HDL cholesterol significantly differ during fat cell differentiation, and that different mechanisms targeting cholesterol to the lipid droplets might exist, depending on its maturation.

MATERIALS AND METHODS

Human plasma HDLs were obtained from Calbiochem, La Jolla, CA. NBD-chol, [22-(*N*-7-nitrobenz-2-oxa-1,3-diazo-4-yl)-amino-23,24-bisnor-5-cholen-3-ol)], LysoTracker Red DND-99, cholera toxin subunit B Alexa Fluor 594 conjugate, monoclonal antibody to Golgin 97, calnexin, BODIPY FLC_5 ceramide, and Alexa Fluor 488 and 546 goat anti-mouse or goat anti-rabbit IgG conjugate were supplied by Molecular Probes (Eugene, OR). Golgi 58K antibody was from Sigma, and monoclonal anti-caveolin-2 IgG antibodies were from Transduction Labs (Lexington, KY). Dulbecco's modified Eagle's medium (DMEM), penicillin/streptomycin, heat-inactivated fetal bovine serum (FBS), and trypsin-EDTA were from Gibco (Invitrogen, France). All other chemicals were from Sigma. A rabbit monoclonal antibody to Rab 6 was supplied by L. Johannes (Institut Curie, France), and a goat monoclonal antibody to the trans-Golgi network (TGN) 38 was supplied by M. Borneins [Institut Curie, France (15)].

Cell culture conditions

3T3-L1 mouse preadipocytes (2×10^4 cells/well) were grown to confluence on either glass coverslips or 8-well Labtek plates (PolyLABO, France) in high-glucose DMEM supplemented with 10% FBS, 20 mM HEPES, and 100 U/ml penicillin/streptomycin. Differentiation of confluent preadipocytes (designated as day 0) was induced by adding methyl-isobutylxanthine (100 μM), dexamethasone (0.25 μM), and insulin (1 μg/ml) to the above solution. After 48 h, the culture medium was replaced with DMEM supplemented with 10% FBS and 1 μg/ml of insulin for 1–12 days. As previously described, cytoplasmic triglyceride droplets were visible by day 4, and 70% to 80% of cells were fully differentiated by day 8 (16). Cells were studied at three different phases of adipocyte differentiation. Phase I comprises days 3–4 after induction of differentiation [i.e., days 1–2 after 1-methyl-3-isobuthylxanthine (MIX)-dexamethasone (DEX) retrieval]. At this stage, no lipid droplets could be observed in the cytoplasm. Phase II and phase III refer to days 7–10 and days 12–14, respectively, after retrieval of MIX-DEX. At these latter phases, cells were fully differentiated and displayed the characteristic lipid droplets of adipocytes.

HDL preparation

HDLs loaded with NBD-chol were reconstituted as described previously (17). In brief, 5 μM NBD-chol was incorporated into human HDL (Calbiochem), and the NBD-chol-loaded HDLs were obtained after ultracentrifugation and extensive dialysis against serum-free culture medium. The protein concentration of NBD-chol-loaded HDL was determined according to Bradford using BSA as a standard (18).

Confocal visualization of NBD-chol uptake and efflux

To assess the uptake and HDL-derived accumulation of NBD-chol, 3T3 adipocytes were incubated in DMEM and 10% lipoprotein-deficient serum (LPDS) at 37°C in the presence of HDL loaded with 5 μM NBD-chol. LPDS was prepared by ultracentrifugation as described elsewhere (12). NBD-chol uptake kinetics were determined using laser confocal fluorescence microscopy on single, living cells. A field on the coverslip chamber containing 10–15 cells was randomly selected, and the position of the microscope objective was focused to view the median section of the cells. Twelve sets were analyzed from a single differentiation. At least five sets of differentiated cultures were recorded for each condition. Cholesterol influx was initiated by addition of NBD-chol and was followed by acquisition of digital images at different time intervals using a time course module (Zeiss AIM software). The average pixel intensity [reactive oxygen intermediates (ROI)] of each single-cell as a function of time was determined using Zeiss software and expressed as mean ± SE. The kinetic of NBD-chol uptake was analyzed by the Marquardt algorithm using UltraFit software from Biosoft (Cambridge, UK). The calculated time constants were analyzed statistically using Student's *t*-test.

Adipose tissue expresses very low levels of ACAT mRNA (19) and virtually no ACAT activity (20). Given that adipocytes have a very low ability to esterify cholesterol, and that 3T3-L1 adipocytes contain essentially free cholesterol (9), intracellular fluorescence is considered to be caused by intact, internalized NBD-chol.

In some experiments, cellular NBD-chol efflux was evaluated as follows: cells were incubated in the presence of HDL NBD-chol (5 μM) for 2 h. Before each efflux experiment, cells were washed three times with DMEM. NBD-chol and efflux kinetics were determined using laser confocal fluorescence microscopy on single, living cells. A field on the coverslip chamber containing 10–15 cells was randomly selected, and the position of the microscope objective was focused to view the median section of the cells. Twelve sets were analyzed from a single differentiation. At least three sets of differentiated cultures were recorded for each condition. Cholesterol efflux was initiated by the addition of cholesterol-free HDL and was followed by acquisition of digital images at different time intervals using a time course module (Zeiss AIM software). The average pixel intensity (ROI) of each single cell as a function of time was determined using Zeiss software and expressed as mean ± SE as described for the uptake experiments. The NBD-chol basal rate was assessed in the absence of HDL and subtracted from that observed in the presence of HDL.

Effects of various pharmacological agents on cholesterol flux and traffic

To study the involvement of cellular energy in the uptake of NBD-chol, 3T3 adipocytes were depleted of their intracellular ATP stores by incubation in glucose-free DMEM with 50 mM deoxyglucose (2 h), 50 μM orthovanadate (90 min), or 3 mM sodium azide (30 min).

To determine whether cholesterol uptake is mediated by the Golgi complex, we assessed NBD-chol uptake in the presence of Brefeldin (2 μg/ml, 30 min) and of monensin (5 μM, 30 min). These compounds are known to disrupt the organization of the Golgi complex and were added for the indicated time before exposure to NBD-chol. The effects of cytochalasin D (20 μM, 60 min), a compound known to disrupt the actin network (21), and *N*-ethyl-maleimide (NEM) (1 mM, 20 min), a V-type ATPase inhibitor (22), on NBD-chol influx were also assessed.

Fluorescent immunochemistry

Cells were grown to confluence on coverslips and differentiated as described above. To assess intracellular NBD-chol distri-

bution, cells were exposed to DMEM containing HDL NBD-chol (5 μg/ml) for 1 h at 37°C. Cells were then washed three times with PBS and fixed with formaldehyde in PBS (3%, 45 min.), followed by exposure to PBS plus glycine (50 mM, 30 min) and then PBS plus BSA (2%, 30 min). Cells were then permeabilized with saponin (0.1%, 5 min) in PBS. For immunolabeling, the cells were incubated in PBS containing one of the following antibodies: Golgi 58K (1:50; v/v), Golgin 97 (1:125; v/v), anti-TGN 38 (1:500; v/v), Rab-6 (1:200; v/v), calnexin (1:200; v/v), and monoclonal antibody 65 anti-caveolin-2 (1:500; v/v). Bound primary antibodies were then visualized with the appropriate Alexa-Fluor (molecular probes) secondary antibodies at a dilution of 1:200 (v/v). Coverslips were mounted onto slides with either VECTASHIELD or SlowFade and observed with a Zeiss laser scanning confocal microscope (LSM 500). Colocalization was quantified as described previously (23).

Labeling of Golgi complex with BODIPY FLC_5 ceramide

Differentiated cells were loaded with 5 μM BODIPY CFL_5 ceramide at 4°C for 15 min, and the medium was then removed and cells washed three times with DMEM solution. The temperature was then increased to 25°C. Immediately thereafter, the live cells were analyzed by fluorescence microscopy.

Fluorescence recovery after photobleaching

To measure the diffusional mobility of NBD-chol in membranes, we used the method of fluorescence recovery after photobleaching (FRAP). In brief, fluorescent molecules in a small area are irreversibly photobleached by an intense laser flash, and fluorescence recovery through the exchange of bleached for nonbleached molecules is measured using low-light illumination. Mobility parameters are then derived from the kinetics of fluorescence recovery, as described previously (24). The mean fluorescence intensities are plotted per area over time, and the experimental data are fitted to the formula for one-dimensional diffusion (equation 1).

$$I_{(t)} = I_{(final)} \{1 - [w^2(w^2 + 4\pi Dt)^{-1}]^{1/2}\} \qquad (Eq.\ 1)$$

where $I_{(t)}$ is the fluorescence intensity as a function of time; zero of time t is taken as the midpoint of the bleach; $I_{(final)}$ is the final intensity reached after complete recovery; W is the strip width; and D is the effective one-dimensional diffusion constant. The diffusion constant D can be obtained directly by spreadsheet programs using least square minimization algorithms. The diffusion constant for NBD-chol was calculated for lipid droplets and cytoplasmic membranes in living cells and compared with that obtained for 2′,7′-bis-(2-carboxyethyl)-5-(6)-carboxyfluorescein (BCECF), a fluorescent probe for intracellular pH. As a control, diffusion of NBD-chol to bleached region was assessed in paraformaldehyde fixed cells. Under these conditions, no recovery of fluorescence should be observed. Recovery was also assessed from the nucleus as a region devoid of a fluorescent probe.

RESULTS

The time course of NBD-chol uptake from HDL best fits a single exponential curve indicative of a first order relationship ($P < 0.001$, a coefficient of determination equal to 0.959, and an F value of 189 (**Fig. 1**). The suitability of a second- and a third-order fit between the fluorescence intensity and time was also analyzed in detail, and in these instances, the P values were 0.51 and 0.80, respectively. First-order kinetic analysis of NBD-chol uptake in cells

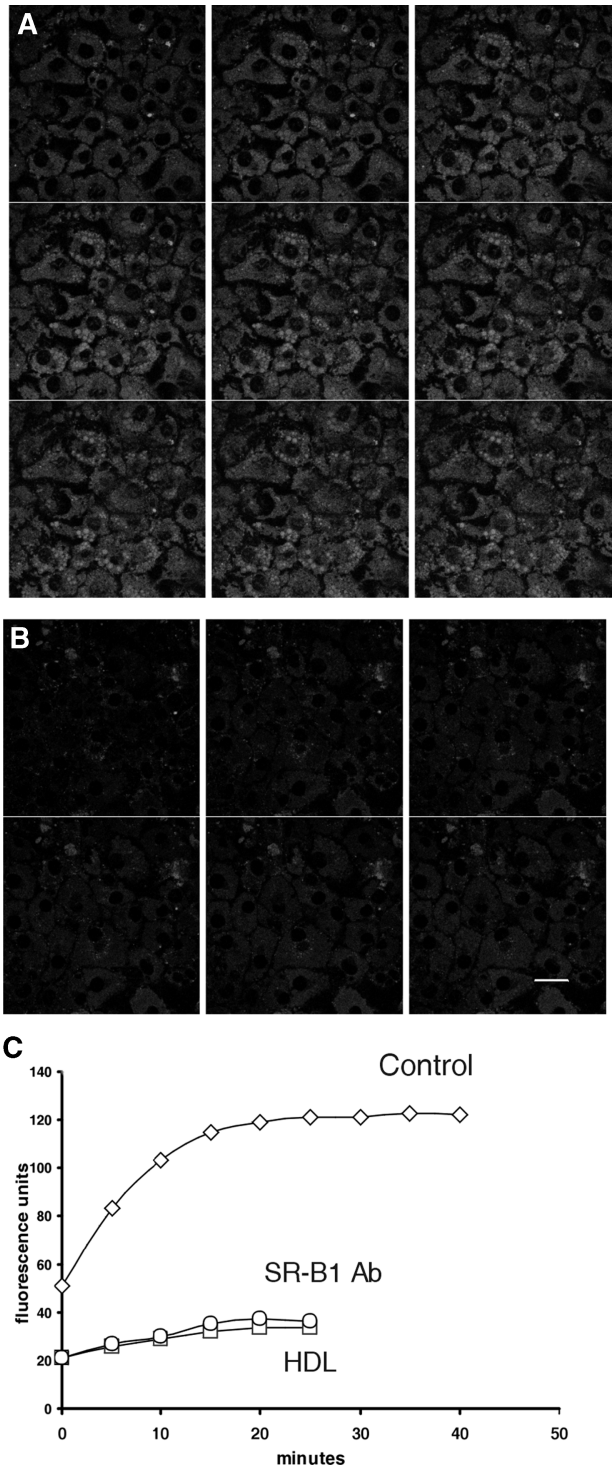

Fig. 1. NBD-cholesterol (NBD-chol) uptake in 3T3-L1 differentiated adipocytes. Single photon excitation images of NBD-chol were collected at 130 s intervals after the addition of HDL-containing NBD-chol to cells in phase II in the absence (A) and presence (B) of a neutralizing antibody to scavenger receptor class B type I (SR-BI) (1:500; v/v). The chronological order is depicted from left to right, top to bottom; bar = 30 μm. The digitized fluorescence signal was corrected for the background fluorescence measured outside the cell. The average fluorescence intensity per cell in control conditions is shown in the presence of unlabeled HDL or antibody to SR-BI antibody (C).

gives a time constant ranging from 0.01–0.09 min^{-1}, with a mean ± SD of 0.036 ± 0.018 min^{-1} (n = 90). Similarly, NBD-chol efflux from cells preloaded with fluorescent lipid followed first order kinetics with a time constant of 0.020 ± 0.010 min^{-1} (mean ± SD). Furthermore, addition of nonlabeled HDL competitively inhibits HDL NBD-chol uptake (Fig. 1C). Similarly, addition of a neutralizing antibody to SR-BI significantly inhibits NBD-chol uptake (Fig.1C). This suggests the involvement of SR-BI in the uptake of HDL-derived NBD-chol.

The distribution of NBD-chol in 3T3-L1 cells largely depends on the phase of differentiation. By 60 min of incubation with NBD-chol, many cells in phase I (with no clearly defined lipid droplets) showed prominent punctuate localizations throughout the cytoplasm (**Fig. 2A**, **B**). In terminally differentiated adipocytes (phases II and III), highly fluorescent lipid droplets could be observed (Fig. 2C–H). The pattern of NBD-chol distribution in these cells resembled that of lipid droplets visible by transmission microscopy (Fig. 2D, F) or stained with Nile red, a selective lipid droplet stain (Fig. 2H).

In order to assess the involvement of cellular energy in the trafficking of cholesterol, cells in phase II were depleted of ATP by incubation with either deoxyglucose, Na-azide, or Na-vanadate. These agents drastically reduced the uptake (**Fig. 3A**) and efflux (data not shown) of NBD-chol. These data establish that HDL-derived cholesterol uptake in adipocytes is an energy-dependent process. On the other hand, cytochalasin D, known to interfere with actin-type filaments, (21) did not significantly modify HDL cholesterol uptake (Fig. 3B).

Intracellular trafficking of NBD-chol

The routes of HDL-derived sterols to the adipocyte lipid droplet are not yet characterized. In this study, we wished to assess the involvement of several cell structures in this trafficking. First, we ensured that under our experimental conditions, the routing of NBD-chol did not follow the lysosomal pathway, which is known to be involved mainly in LDL uptake. To this end, cells were labeled with LysoTracker Red, and NBD-chol uptake from HDL was followed for a period of 60 min. No colocalization of cholesterol within lysosomes could be observed during this time interval. **Figure 4** depicts lysosomal distribution (Fig. 4A) and NBD-chol (Fig. 4B) at 60 min after initiation of NBD-chol uptake, with no colocalization between these two fluorescent dyes (Fig. 4D). These results suggest that uptake and routing of sterol from HDL follows a pathway different from that of LDL.

We next wished to determine the role of the Golgi complex in the uptake, intracellular transport, and storage of HDL-derived NBD-chol in adipocytes. Cells were pretreated with several agents known to disrupt Golgi function and structure. These include Brefeldin A (BFA) (25) and monensin, which disorganize the Golgi complex. As shown in Fig. 3B, treatment with BFA or monensin drastically reduced cholesterol uptake by these cells, thus implicating the Golgi complex in this process and possibly in intracellular trafficking. A similar reduction in the rate of

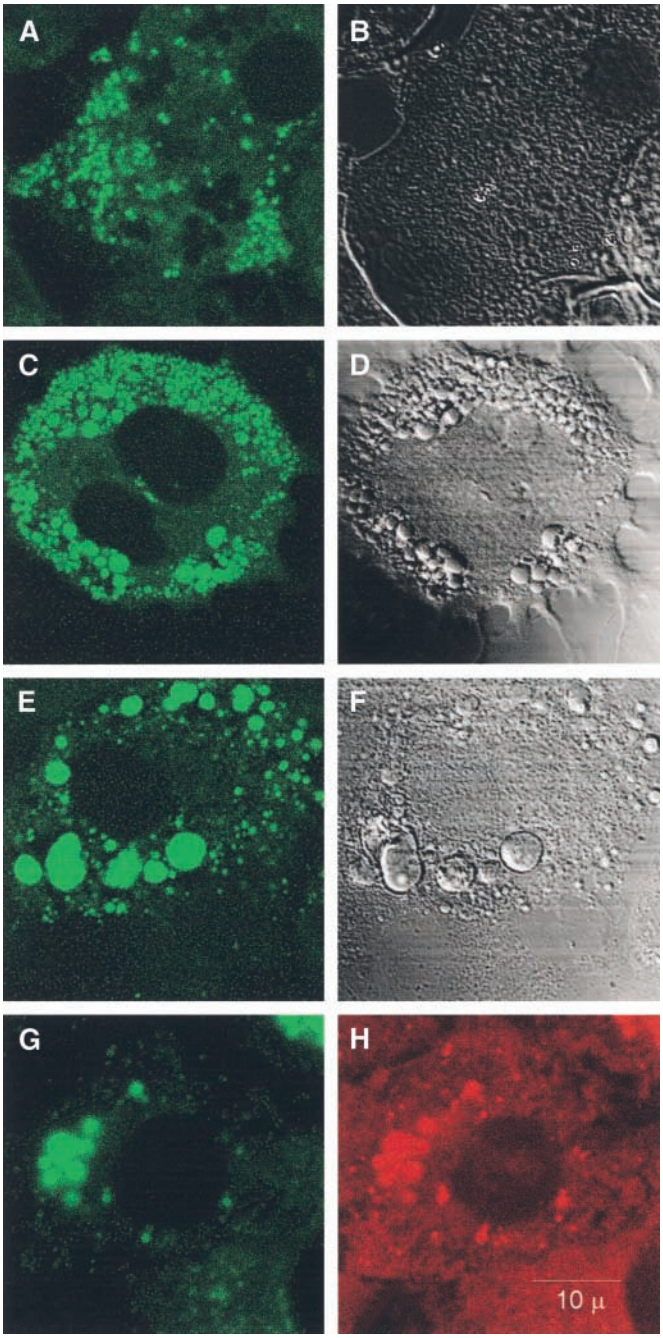

Fig. 2. NBD-chol distribution in 3T3-L1 adipocytes during differentiation. Cells were incubated with HDL loaded with NBD-chol for 1 h and examined by confocal microscopy at three different phases of adipocyte differentiation: phase I (A, B) at days 3 to 4 after induction of differentiation [i.e., days 1 to 2 after 1-methyl-3-isobuthylxanthine (MIX)-dexamethasone (DEX) retrieval]. At this stage, no lipid droplets could be observed in the cytoplasm. Phase II (C, D) and phase III (E, F) are shown at days 7 to 10 and days 12 to 14, respectively, after retrieval of MIX-DEX. At these latter phases, cells were fully differentiated and displayed the characteristic lipid droplets of adipocytes. A, C, E: Single photon excitation images of NBD-chol fluorescence. B, D, F: Transmitted light images of cell. Double labeling of cells depicted at phase III with NBD-chol (G) and Nile red (H). Single-cell distribution of NBD-chol representative of more than 100 individual cells was examined in at least 30 experiments; bar = 10 μm.

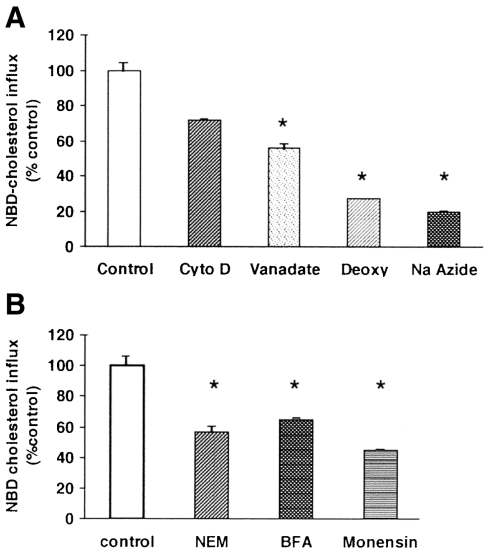

Fig. 3. Effect of pharmacological agents on uptake of HDL-mediated NBD-chol. 3T3-L1 cells were grown as described in Materials and Methods. A: Differentiated cells in phase II were pretreated with cytochalasin D (20 μM, 60 min) in DMEM or incubated in a glucose-free DMEM with vanadate (50 μM, 90 min), deoxyglucose (50 mM, 2 h), or sodium azide (3 mM, 30 min). B: Differentiated cells in phase II were pretreated with *N*-ethyl-maleimide (1 mM, 20 min), Brefeldin A (2 μg/ml, 30 min), and monensin (5 μM, 30 min). After pretreatment with pharmacological agents, cells were incubated in lipoprotein-deficient serum (LPDS)/DMEM containing NBD-chol-loaded HDL, and uptake was recorded at regular time intervals. Time constant was calculated after fitting with first-order kinetics. Results (mean value ± SD, $n \geq 5$) are expressed as percent of untreated cells. * *t*-test control versus treated cells, $P \leq 0.05$.

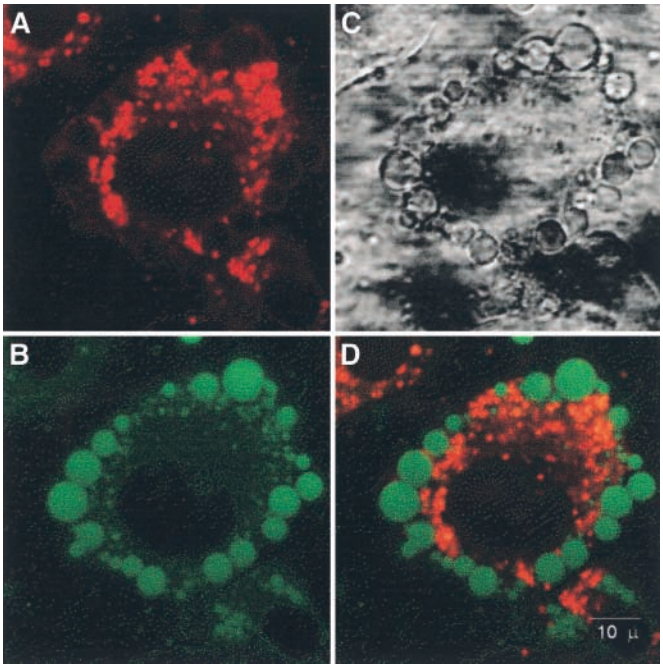

Fig. 4. Intracellular localization of NBD-chol in adipocytes dually labeled with NBD-chol and LysoTracker Red. Cells in phase III were incubated in LPDS/DMEM in the presence of HDL NBD-chol and LysoTracker Red DND-99 (molecular probes) for 1 h at 37°C. LysoTracker Red was excited with 543 nm laser line and emission was detected with a 580 long path filter (A). NBD-chol was excited with the 488 nm laser line and fluorescence emission detected with a 505–530 band path filter (B). Transmitted light image was obtained with a Zeiss laser scanning microscope (C). Colocalization (D); bar = 10 μm.

NBD-chol uptake was observed with NEM (Fig. 3B), reported to inhibit the NEM-sensitive factor involved in the transport of molecules from the TGN to other cell organelles (26).

We next assessed the colocalization of NBD-chol with the Golgi complex using antibodies to Golgin 97. Interestingly, in phase I, when no visible lipid droplets have yet accumulated in cells, fluorescent labeling with antibody to Golgin 97 revealed a dispersed Golgi complex spread all over the cytoplasm, and NBD-chol was found to be colocalized within these Golgi structures (**Fig. 5A–C**). The percent of cholesterol colocalized with Golgi (chol/Golgi) in phase I was 86% while that of Golgi/chol was 57% (Fig. 5C). In phase II, antibody to Golgin 97 was dispersed in the cytoplasm, and NBD-chol was localized in nascent lipid droplets and cytoplasm. (Fig. 5D–E). Whereas the Golgi complex formed a compact juxtanuclear structure in phase III cells (Fig. 5G–I), NBD-chol is present primarily in lipid droplets (Fig. 5H) with no colocalization (Fig. 5I).

In order to further establish the scattering of the Golgi complex in phase I, we used either a live marker of the Golgi complex (BODIPY FLC_5 ceramide) or several antibodies to Golgi markers: Golgi 58K, Rab 6, or TGN 38. As shown in **Fig. 6**, a scattered pattern of all of these antibodies was observed in the cytoplasm, strongly suggesting a dispersed Golgi complex in cells in phase I of the differentiation process (Fig. 6A–C). Similar patterns were obtained using BODIPY ceramide in living cells (Fig. 6D), thus validating the distribution observed by immunofluorescence in fixed cells. This markedly differs from the juxtanuclear location of the Golgi complex in phase III cells with prominent lipid droplets (see Figs. 5G, 6E). Projections of confocal serial sections of cells in phase I showed that the different fluorescent Golgi markers were scattered over the entire volume of the cell, excluding the nucleus, and were colocalized with NBD-chol (data not shown). These data establish that the distribution of Golgi complex exhibits marked changes during the differentiation process. A dispersed distribution colocalized with cholesterol was observed in phase I, whereas in fully differentiated lipid laden cells, cholesterol segregates from the juxtanuclear Golgi complex and distributes preferentially in lipid droplets.

Labeling of caveolin-2

Caveolins are cholesterol binding proteins and have been shown to be distributed mainly at the plasma membrane and also in the Golgi complex. They exist as three distinct isoforms, caveolin-2 being the most abundant subtype in adipocytes (27, 28). In order to further document the differential localization of cholesterol and Golgi markers during the course of adipocyte differentiation, we stained cells for caveolin-2. In phase I cells, endogenous caveolin-2 was detected by immunostaining with a monoclonal an-

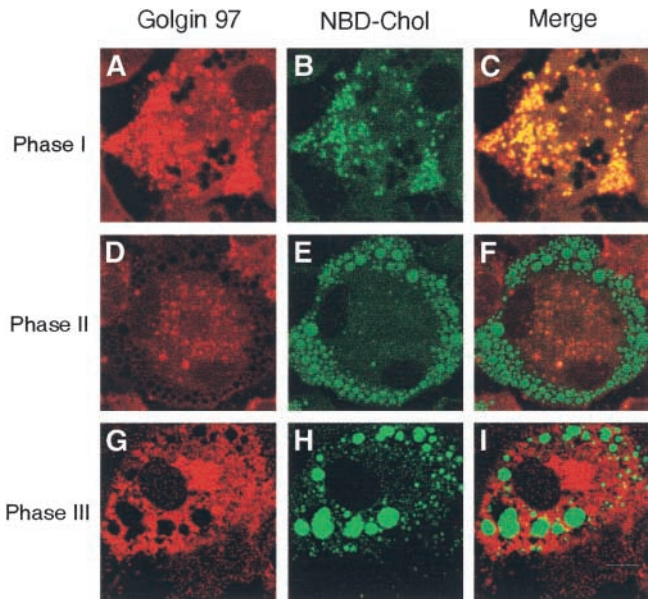

Fig. 5. Double-label immunofluorescence with Golgi marker and NBD-chol. Typical example of cells at phase I (A–C), phase II (D–F), and phase III (G–I) of differentiation were simultaneously labeled for Golgin 97 with Alexa-Fluor 546 conjugated goat anti-mouse IgG (A, D, G) and NBD-chol (B, E, H). Colocalization (C, F, I) was shown using pseudo-coloring, resulting in yellow to orange where superimposition occurred. Bar = 10 μm.

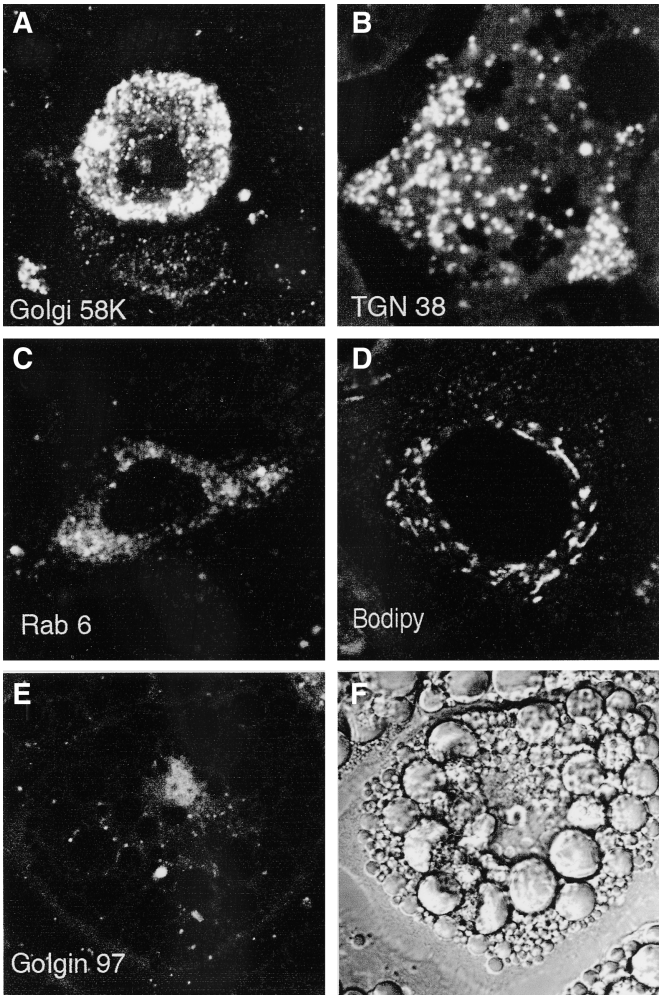

Fig. 6. Intracellular distribution of Golgi markers in adipocytes at different phases of differentiation. 3T3-L1 cells were differentiated with MIX, DEX, and insulin as described in Materials and Methods. Cells at phase I (A–D) of differentiation were analyzed by immunofluorescence and laser confocal microscopy. Note the widespread distribution in the cytoplasm of Golgi 58K (A), trans-Golgi network (TGN) 38 (B), Rab 6 (C), and BODIPY FLC_5 ceramide (D) at phase I. Cells depicted at phase III are labeled with Golgin 97 (E), and fully formed lipid droplets could be observed with phase-contrast microscopy (F). One of at least 10 experiments gave similar results. Bar = 10 μm.

tibody against human caveolin-2 (mAb 65), exhibiting a scattered distribution and colocalizing with NBD-chol (**Fig. 7A–C**). During later phases, NBD-chol was mainly present in lipid droplets while caveolin-2 exhibited a marked juxtanuclear distribution and was also observed at the cell membrane (Fig. 7D–F). Thus, the distribution of caveolin-2 at different phases resembles that of Golgi markers.

Lateral mobility of NBD-chol

Because NBD-chol was found to be distributed throughout the cytoplasm and colocalized with the Golgi complex in cells at phase I, we wished to assess whether the probe was integrated to membranous elements rather than clustered in micelles in the cytosol. Fluorescent recovery after photobleaching was used to measure the rate at which NBD-chol diffused into photobleached areas. **Figure 8** depicts FRAP of NBD-chol. Outlined areas were irreversibly photobleached by an intense laser flash, and fluorescence recovery through exchange of bleached for nonbleached molecules was assessed in the cytoplasm and in lipid droplets. As a control, an area of the nucleus devoid of NBD-chol was also photobleached. The value of diffusion constant (Fig. 8D) was calculated as described in the Materials and Methods. The mean value of $D \pm$ SD in the cytoplasm was $0.13 \pm 0.12 \times 10^{-8}$ cm^2 sec^{-1}. When calculated separately for lipid droplets, it was $0.08 \pm 0.06 \times 10^{-8}$ cm^2 sec^{-1} and $0.46 \pm 0.32 \times 10^{-8}$ cm^2 sec^{-1} for cytoplasm ($P \leq 0.05$, n = 8). These values are of a magnitude similar to those observed for membrane-integrated elements, such as NBD-phosphatidylserine, NBD-phosphatidylcholine, neutral lipids, cholecytokinin, or laminin receptor (24, 29–31). In contrast, recovery from photobleaching of BCECF was instantaneous (10^5 cm^2 sec^{-1}) in accordance with values obtained for diffusion of molecules in liquid phase (data not shown). As expected, no recovery could be observed in formaldehyde-fixed cells, which blocked the movement of the probe (data not shown), or in the nucleus, which was devoid of a fluorescent probe.

DISCUSSION

In this study, we wished to investigate the intracellular routes through which exogenous cholesterol is targeted to lipid droplets in an adipocyte cell. For this purpose we

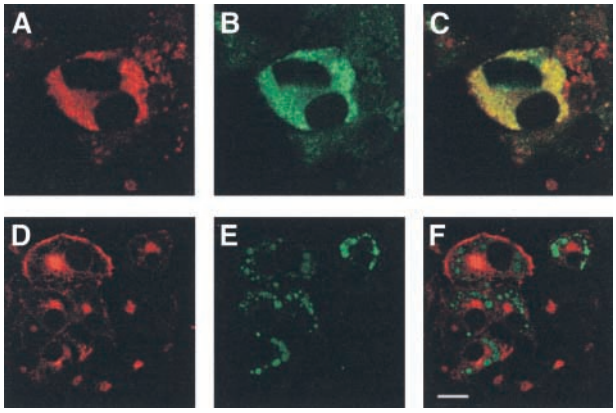

Fig. 7. Double-label immunofluorescence with caveolin-2 and NBD-chol. Cells at phase I (A–C) and III (D–F) of differentiation were simultaneously labeled for NBD-chol (B, E) and caveolin-2 with Alexa-Fluor 546-conjugated goat anti-mouse IgG (A, D). Colocalization (C, F) was shown using pseudo-coloring resulting in yellow to orange where superimposition occurred. Bar = 10 μm.

used a dynamic cell system in which fibroblast-like cells differentiate to lipid-filled mature adipocytes.

Interestingly, the results of the present investigation provide novel evidence for differential localization of Golgi markers, caveolin-2, and NBD-chol during the fat cell differentiation process. On the other hand, influx of HDL-derived NBD-chol into adipocytes is an efficient, ATP-dependent process that requires a functional Golgi apparatus.

This study shows that in 3T3-L1 adipocytes, the uptake of NBD-chol from HDL requires SR-BI, as an antibody to this latter significantly inhibits this uptake. This receptor functions as a docking receptor for HDL, is highly expressed in cells, and was found to promote the selective uptake of HDL cholesterol esters to cells (13, 14). Once internalized by differentiated fat cells, NBD-chol rapidly distributes throughout the cytoplasm and targets lipid droplets through a route that is independent of lysosomes. This targeting requires a functional Golgi apparatus, as it is inhibited by BFA, monensin, and NEM, all known to disorganize the Golgi complex, and is an ATP-dependent process.

One novel and salient feature of the present study is that during the early phase of adipose maturation, a unique distribution of Golgi markers, caveolin-2, and NBD-chol occurs, clearly distinct from that observed in mature fat cells (i.e., with fully formed lipid vesicles). Thus, in the very first days following fat cell differentiation in cells without visible lipid droplets, a scattering of the Golgi apparatus across the cytoplasm is observed using different antibodies to Golgi structures (TGN 38, Rab 6, Golgin 97, and Golgi 58K). Similar results were obtained in living cells using BODIPY-ceramide. Furthermore, NBD-chol was found to be colocalized with the widespread Golgi structure. Similarly, in the first phase of differentiation, caveolin-2 showed a scattered cytoplasmic distribution and a high colocalization with NBD-chol. At a later stage, when lipid droplets are fully formed, NBD-chol gradually concentrates in these droplets, while the Golgi complex shows an expected juxtanuclear localization. Caveolin-2 labeling also concentrates near the nucleus, probably in the Golgi complex.

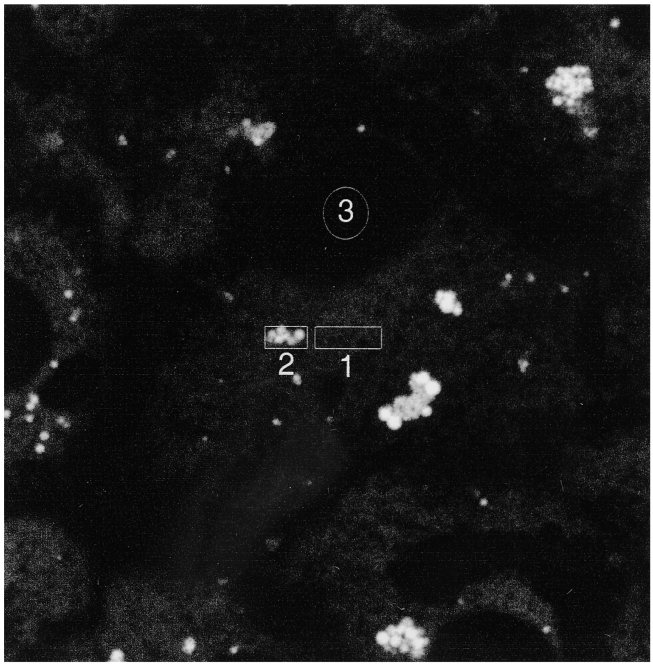

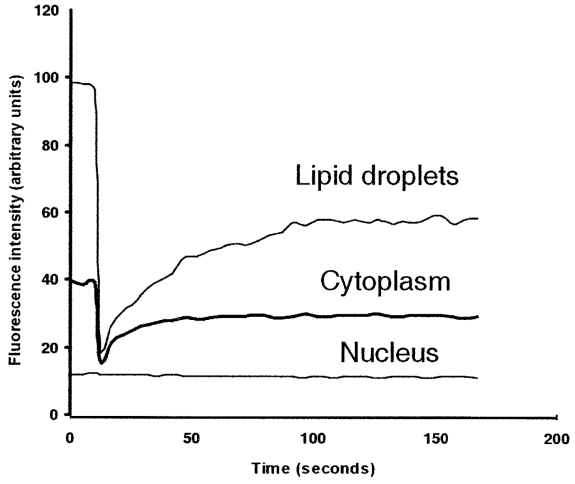

Fig. 8. Fluorescence recovery after photobleaching experiment of NBD-chol (A) and 2′,7′-bis-(2-carboxyethyl)-5-(and 6)-carboxyfluorescein (B) in 3T3-L1 cells. A cell at phase II of differentiation, loaded with NBD-chol, was imaged with an attenuated laser on a confocal laser-scanning microscope. One image was taken prior to the photobleach during which the outlined box was then illuminated with full laser power. Immediately after the bleach, the cell was imaged again with low-light levels until recovery was complete. Calculated fluorescence intensity in the bleached strip before and after photobleach is plotted against time for the cytoplasm (1), lipid droplet (2), and NBD-chol-free nucleus (3), and is inhibited in the presence of unloaded HDL. A neutralizing SR-BI antibody with partially inhibited cholesterol uptake and distribution to lipid vesicles, together with the fact that HDL-mediated NBD-chol does not colocalize with lysosomes and its influx is inhibited, strongly suggests that this uptake is different from that specific to LDL.

Golgi stacks were reported to break down and reform during vertebrate mitosis (32–34). In several cell types, the process of Golgi dispersal and reaggregation occurs within hours during cell division; however, in the present study in 3T3-L1 differentiated cells, the scattering is present for several days, suggesting that it might not be related to mitosis per se. The adipocyte differentiation program is known to involve several distinct phases. As preadipocytes reach confluence, they enter a temporary quiescent state that appears to be a prerequisite for subsequent differentiation. This cell cycle arrest, however, is overcome by mitotic and adipogenic inducers. Thus, upon addition of the differentiation inducers, i.e., a combination of isobutylmethylxanthine, dexamethasone, and a high level of insulin, the cells reenter the cell cycle and undergo two to three rounds of mitosis, referred to as mitotic clonal expansion (35). Several studies have reported that cell division in 3T3-L1 occurs during the first 48 h after induction of differentiation (i.e., after addition of MIX-DEX insulin) (36–38). The results presented in this study show that the dispersal of Golgi elements in phase I is observed at days 1 through 4 after retrieval of adipogenic agents. This long-lasting event is unlikely to be concomitant to mitosis or clonal expansion per se, however; the cell cycle stages need to be assessed before reaching any definitive conclusion.

The role of the fragmentation of the Golgi in cell biological processes is yet unclear. The colocalization of NBD-chol with the Golgi elements at the first phase of adipocyte differentiation, together with the inhibitory effect on NBD-chol influx of monensin, Brefeldin, and NEM, strongly suggests that the Golgi participate in the traffic and routing of cholesterol to lipid droplets. A number of studies have suggested that the Golgi apparatus has an important role in regulating intracellular cholesterol homeostasis. For instance, the Golgi apparatus contributes to the transport of endogenously synthesized cholesterol enroute to the plasma membrane (4). Other studies indicate that the Golgi apparatus is involved in apolipoprotein-mediated cholesterol efflux (6, 7). Finally, recent studies indicate that LDL-derived cholesterol is transported from clathrin-coated vesicles into intermediate-density vesicles that contain markers for the TGN before reaching plasma membrane caveolae (5). The present study shows novel data suggesting that the Golgi elements could play a major role in NBD-chol uptake from HDL, and possibly their trafficking to the lipid droplets. Whether scattering of the Golgi elements is required for or does participate in lipid vesicle formation deserves further investigation.

NBD-chol was reported to be a useful probe for monitoring HDL-mediated cholesterol influx and efflux (39, 40); however, some concerns have been raised about the ability of NBD-chol to mimic natural cholesterol distribution (41, 42). In this regard, Mukherjee et al. reported that NBD-chol and dehydroergosterol (DHE), a naturally occurring fluorescent sterol, distribute differently in Chinese hamster ovary cells (42). In contrast, Frolov et al. reported a similar distribution of these two fluorescent probes in L fibroblasts (40). In addition, NBD-chol traffics by similar uptake as well as secretory pathways in L cell fibroblasts and CaCo2 cells (10, 39, 40, 43). In this study, control experiments showed a similar distribution in the cytoplasm of DHE and NBD-chol (data not shown). On the other hand, several factors were reported to determine the incorporation of fluorescent sterols to membranes. The thickness and curvature of reconstituted membranes affected the incorporation of NBD-chol in these structures (44). While the mode of delivery of DHE to the cell determined its incorporation to plasma membranes (45), to our knowledge there is yet no fluorescent analog that exactly reflects native cholesterol distribution and metabolism. There are clearly limitations to the use of NBD-chol, but this probe offers some desirable properties, and one should be careful before drawing conclusions concerning native cholesterol.

Caveolin directly binds cholesterol and represents the major structural component of caveolae in vivo (27, 28). It has been proposed that caveolins participate in vesicular trafficking events and signal transduction processes by acting as scaffolding proteins to organize and concentrate cholesterol and glycosphingolipids within caveolar membranes (46). Lipid rafts are organized mainly at the level of the plasma membrane, but they can also form within internal membrane compartments, such as the Golgi apparatus (47). Furthermore, there is compelling evidence that caveolin-1 and caveolin-2 are present at the Golgi complex (48–50). Our results are in accord with this scheme, as caveolin 2 colocalizes with NBD-chol and is scattered all over the cytoplasm in the first phase of adipocyte formation. At later phases of adipocyte formation, it concentrates at a juxtanuclear location in what resembles the Golgi complex.

Recently, lipid rafts and caveolae have received much attention as potential regulators and organizing centers for signal transduction and membrane trafficking pathways. In this regard, Fujimoto et al. reported that caveolin-2 is targeted to the surface of lipid droplets (51). These results suggest that lipid droplets are involved in the trafficking of cholesterol molecules mediated by caveolins. Ostermeyer et al. obtained similar results and postulated that ER targeting or ER retention of caveolin-1 allows caveolin-1 to be rerouted to lipid droplets, thereby preventing its accumulation within caveolae at the level of the plasma membrane (52). This is of particular interest in regard to our present data, which point out that targeting of cholesterol to the lipid droplets in the initial phase of their formation involves a scattering process of the Golgi apparatus. Whether the initial routing of NBD-chol to lipid droplets from the disrupted Golgi apparatus requires transit via the ER was not addressed in this study. Several insights into HDL-mediated cholesterol uptake and trafficking have been obtained over the past few years; however, the mechanisms for these pathways have yet to be elucidated [as reviewed in ref. (53)].

In conclusion, this study points out distinct routing mechanisms of HDL-derived cholesterol in the early and late phases of adipocyte formation in which the structure

of the Golgi complex plays a critical role. To what extent such changes in the distribution of the Golgi apparatus might participate, from cholesterol localization to the forming of lipid droplets, remains to be established.

The authors wish to thank Dr. Ludger Johannes (Institut Curie) for fruitful discussions.

REFERENCES

1. Simons, K., and D. Toomre. 2000. Lipid rafts and signal transduction. *Nat. Rev. Mol. Cell Biol.* **1:** 31–39.
2. Goldstein, J. L., and M. S. Brown. 1990. Regulation of the mevalonate pathway. *Nature.* **343:** 425–430.
3. Brown, M. S., and J. L. Goldstein. 1997. The SREBP pathway: regulation of cholesterol metabolism by proteolysis of a membrane-bound transcription factor. *Cell.* **89:** 331–340.
4. Anderson, R. G., and R. K. Pathak. 1985. Vesicles and cisternae in the trans Golgi apparatus of human fibroblasts are acidic compartments. *Cell.* **40:** 635–643.
5. Fielding, P. E., and C. J. Fielding. 1996. Intracellular transport of low density lipoprotein derived free cholesterol begins at clathrin-coated pits and terminates at cell surface caveolae. *Biochemistry.* **35:** 14932–14938.
6. Mendez, A., and L. Uint. 1996. Apolipoprotein-mediated cellular cholesterol and phospholipid efflux depend on a functional Golgi apparatus. *J. Lipid Res.* **37:** 2510–2524.
7. Mendez, A. J. 1995. Monensin and Brefeldin A inhibit high density lipoprotein-mediated cholesterol efflux from cholesterol-enriched cells. *J. Biol. Chem.* **270:** 5891–5900.
8. Murphy, D. J. 2001. The biogenesis and functions of lipid bodies in animals, plants and microorganisms. *Prog. Lipid Res.* **40:** 325–438.
9. Le Lay, S., C. Robichon, X. Le Liepvre, G. Dagher, P. Ferre, and I. Dugail. 2003. Regulation of ABCA1 expression and cholesterol efflux during adipose differentiation of 3T3–L1 cells. *J. Lipid Res.* **44:** 1499–1507.
10. Prattes, S., G. Horl, A. Hammer, A. Blaschitz, W. F. Graier, W. Sattler, R. Zechner, and E. Steyrer. 2000. Intracellular distribution and mobilization of unesterified cholesterol in adipocytes: triglyceride droplets are surrounded by cholesterol-rich ER-like surface layer structures. *J. Cell Sci.* **113:** 2977–2989.
11. Boizard, M., X. Le Liepvre, P. Lemarchand, F. Foufelle, P. Ferre, and I. Dugail. 1998. Obesity-related overexpression of fatty-acid synthase gene in adipose tissue involves sterol regulatory element-binding protein transcription factors. *J. Biol. Chem.* **273:** 29164–29171.
12. Le Lay, S., S. Krief, C. Farnier, I. Lefrere, X. Le Liepvre, R. Bazin, P. Ferre, and I. Dugail. 2001. Cholesterol, a cell size-dependent signal that regulates glucose metabolism and gene expression in adipocytes. *J. Biol. Chem.* **276:** 16904–16910.
13. Babitt, J., B. Trigatti, A. Rigotti, E. J. Smart, R. G. Anderson, S. Xu, and M. Krieger. 1997. Murine SR-BI, a high density lipoprotein receptor that mediates selective lipid uptake, is N-glycosylated and fatty acylated and colocalizes with plasma membrane caveolae. *J. Biol. Chem.* **272:** 13242–13249.
14. Graf, G. A., P. M. Connell, D. R. van der Westhuyzen, and E. J. Smart. 1999. The class B, type I scavenger receptor promotes the selective uptake of high density lipoprotein cholesterol ethers into caveolae. *J. Biol. Chem.* **274:** 12043–12048.
15. Jasmin, B. J., J. Cartaud, M. Bornens, and J. P. Changeux. 1989. Golgi apparatus in chick skeletal muscle: changes in its distribution during end plate development and after denervation. *Proc. Natl. Acad. Sci. USA.* **86:** 7218–7222.
16. Hwang, C-S., T. M. Loftus, S. Mandrup, and M. D. Lane. 1997. Adipocyte differentiation and leptin expression. *Annu. Rev. Cell Dev. Biol.* **13:** 231–259.
17. Pitas, R. E., T. L. Innerarity, J. N. Weinstein, and R. W. Mahley. 1981. Acetoacetylated lipoproteins used to distinguish fibroblasts from macrophages in vitro by fluorescence microscopy. *Arteriosclerosis.* **1:** 177–185.
18. Bradford, M. M. 1976. A rapid and sensitive method for the quantitation of microgram quantities of protein utilizing the principle of protein-dye binding. *Anal. Biochem.* **72:** 248–254.
19. Uelmen, P. J., K. Oka, M. Sullivan, C. C. Y. Chang, T. Y. Chang, and L. Chan. 1995. Tissue-specific expression and cholesterol regulation of acylcoenzyme A:cholesterol acyltransferase (ACAT) in mice. *J. Biol. Chem.* **270:** 26192–26201.
20. Little, M. T., and P. Hahn. 1992. Ontogeny of acyl-CoA: cholesterol acyltransferase in rat liver, intestine, and adipose tissue. *Am. J. Physiol.* **262:** G599–G602.
21. Yahara, I., F. Harada, S. Sekita, K. Yoshihira, and S. Natori. 1982. Correlation between effects of 24 different cytochalasins on cellular structures and cellular events and those on actin in vitro. *J. Cell Biol.* **92:** 69–78.
22. Stone, D. K., and X. S. Xie. 1988. Proton translocating ATPases: issues in structure and function. *Kidney Int.* **33:** 767–774.
23. Manders, E. E. M., F. J. Verbeek, and J. A. Aten. 1993. Measurement of co-localisation of objects in dual-colour confocal images. *J. Microscopy.* **169:** 375–382.
24. Ellenberg, J., and J. Lippincott-Schwartz. 1999. Dynamics and mobility of nuclear envelope proteins in interphase and mitotic cells revealed by green fluorescent protein chimeras. *Methods.* **19:** 362–372.
25. Pelham, H. R. 1991. Multiple targets for Brefeldin A. *Cell.* **67:** 449–451.
26. Ikonen, E., M. Tagaya, O. Ullrich, C. Montecucco, and K. Simons. 1995. Different requirements for NSF, SNAP, and Rab proteins in apical and basolateral transport in MDCK cells. *Cell.* **81:** 571–580.
27. Razani, B., and M. P. Lisanti. 2001. Caveolins and caveolae: molecular and functional relationships. *Exp. Cell Res.* **271:** 36–44.
28. Schlegel, A., and M. P. Lisanti. 2001. The caveolin triad: caveolae biogenesis, cholesterol trafficking, and signal transduction. *Cytokine Growth Factor Rev.* **12:** 41–51.
29. Cezanne, L., A. Lopez, F. Loste, G. Parnaud, O. Saurel, P. Demange, and J. F. Tocanne. 1999. Organization and dynamics of the proteolipid complexes formed by annexin V and lipids in planar supported lipid bilayers. *Biochemistry.* **38:** 2779–2786.
30. Fulbright, R. M., D. Axelrod, W. R. Dunham, and C. L. Marcelo. 1997. Fatty acid alteration and the lateral diffusion of lipids in the plasma membrane of keratinocytes. *Exp. Cell Res.* **233:** 128–134.
31. Roettger, B. F., D. I. Pinon, T. P. Burghardt, and L. J. Miller. 1999. Regulation of lateral mobility and cellular trafficking of the CCK receptor by a partial agonist. *Am. J. Physiol.* **276:** C539–C547.
32. Lippincott-Schwartz, J., and K. J. Zaal. 2000. Cell cycle maintenance and biogenesis of the Golgi complex. *Histochem. Cell Biol.* **114:** 93–103.
33. Ralston, E. 1993. Changes in architecture of the Golgi complex and other subcellular organelles during myogenesis. *J. Cell Biol.* **120:** 399–409.
34. Zaal, K. J., C. L. Smith, R. S. Polishchuk, N. Altan, N. B. Cole, J. Ellenberg, K. Hirschberg, J. F. Presley, T. H. Roberts, E. Siggia, R. D. Phair, and J. Lippincott-Schwartz. 1999. Golgi membranes are absorbed into and reemerge from the ER during mitosis. *Cell.* **99:** 589–601.
35. MacDougald, O. A., and M. D. Lane. 1995. Transcriptional regulation of gene expression during adipocyte differentiation. *Annu. Rev. Biochem.* **64:** 345–373.
36. Jin, S., B. Zhai, Z. Qiu, J. Wu, M. D. Lane, and K. Liao. 2000. c-Crk, a substrate of the insulin-like growth factor-1 receptor tyrosine kinase, functions as an early signal mediator in the adipocyte differentiation process. *J. Biol. Chem.* **275:** 34344–34352.
37. Patel, Y. M., and M. D. Lane. 2000. Mitotic clonal expansion during preadipocyte differentiation: calpain-mediated turnover of p27. *J. Biol. Chem.* **275:** 17653–17660.
38. Qiu, Z., Y. Wei, N. Chen, M. Jiang, J. Wu, and K. Liao. 2001. DNA synthesis and mitotic clonal expansion is not a required step for 3T3–L1 preadipocyte differentiation into adipocytes. *J. Biol. Chem.* **276:** 11988–11995.
39. Atshaves, B. P., O. Starodub, A. McIntosh, A. Petrescu, J. B. Roths, A. B. Kier, and F. Schroeder. 2000. Sterol carrier protein-2 alters high density lipoprotein-mediated cholesterol efflux. *J. Biol. Chem.* **275:** 36852–36861.
40. Frolov, A., A. Petrescu, B. P. Atshaves, P. T. C. So, E. Gratton, G. Serrero, and F. Schroeder. 2000. High density lipoprotein-mediated cholesterol uptake and targeting to lipid droplets in intact L-cell fibroblasts. A single- and multiphoton fluorescence approach. *J. Biol. Chem.* **275:** 12769–12780.
41. Loura, L. M., A. Fedorov, and M. Prieto. 2001. Exclusion of a cholesterol analog from the cholesterol-rich phase in model membranes. *Biochim. Biophys. Acta.* **1511:** 236–243.

42. Mukherjee, S., X. Zha, I. Tabas, and F. R. Maxfield. 1998. Cholesterol distribution in living cells: fluorescence imaging using dehydroergosterol as a fluorescent cholesterol analog. *Biophys. J.* **75:** 1915–1925.
43. Sparrow, C. P., S. Patel, J. Baffic, Y-S. Chao, M. Hernandez, M-H. Lam, J. Montenegro, S. D. Wright, and P. A. Detmers. 1999. A fluorescent cholesterol analog traces cholesterol absorption in hamsters and is esterified in vivo and in vitro. *J. Lipid Res.* **40:** 1747–1757.
44. Rukmini, R., S. S. Rawat, S. C. Biswas, and A. Chattopadhyay. 2001. Cholesterol organization in membranes at low concentrations: effects of curvature stress and membrane thickness. *Biophys. J.* **81:** 2122–2134.
45. McIntosh, A. L., A. M. Gallegos, B. P. Atshaves, S. M. Storey, D. Kannoju, and F. Schroeder. 2003. Fluorescence and multiphoton imaging resolve unique structural forms of sterol in membranes of living cells. *J. Biol. Chem.* **278:** 6384–6403.
46. Anderson, R. G. 1998. The caveolae membrane system. *Annu. Rev. Biochem.* **67:** 199–225.
47. Gkantiragas, I., B. Brugger, E. Stuven, D. Kaloyanova, X. Y. Li, K. Lohr, F. Lottspeich, F. T. Wieland, and J. B. Helms. 2001. Sphingomyelin-enriched microdomains at the Golgi complex. *Mol. Biol. Cell.* **12:** 1819–1833.
48. Luetterforst, R., E. Stang, N. Zorzi, A. Carozzi, M. Way, and R. G. Parton. 1999. Molecular characterization of caveolin association with the Golgi complex: identification of a cis-Golgi targeting domain in the caveolin molecule. *J. Cell Biol.* **145:** 1443–1459.
49. Machleidt, T., W-P. Li, P. Liu, and R. G. W. Anderson. 2000. Multiple domains in caveolin-1 control its intracellular traffic. *J. Cell Biol.* **148:** 17–28.
50. Mora, R., V. L. Bonilha, A. Marmorstein, P. E. Scherer, D. Brown, M. P. Lisanti, and E. Rodriguez-Boulan. 1999. Caveolin-2 localizes to the Golgi complex but redistributes to plasma membrane, caveolae, and rafts when co-expressed with caveolin-1. *J. Biol. Chem.* **274:** 25708–25717.
51. Fujimoto, T., H. Kogo, K. Ishiguro, K. Tauchi, and R. Nomura. 2001. Caveolin-2 is targeted to lipid droplets, a new "membrane domain" in the cell. *J. Cell Biol.* **152:** 1079–1085.
52. Ostermeyer, A. G., J. M. Paci, Y. Zeng, D. M. Lublin, S. Munro, and D. A. Brown. 2001. Accumulation of caveolin in the endoplasmic reticulum redirects the protein to lipid storage droplets. *J. Cell Biol.* **152:** 1071–1078.
53. Mukherjee, S., and F. R. Maxfield. 2000. Role of membrane organization and membrane domains in endocytic lipid trafficking. *Traffic.* **1:** 203–211.